BOLETIN DE LA SOCIEDAD ESPAÑOLA DE
Cerámica y Vidrio
www.elsevier.es/bsecv

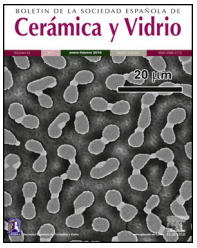

The role of Tb_2O_3 in enhancement the properties of the La_2O_3–P_2O_5 glass system: Mechanical and radiation shielding study

Aljawhara H. Almuqrin[a], *Mohamed Y. Hanfi*[b,c], *Mohammed I. Sayyed*[d,e], *Karem Mahmoud*[b,c,*], *Hanan Al-Ghamdi*[a], *Dalal Abdullah Aloraini*[a], *Badriah Albarzan*[a]

[a] *Department of Physics, College of Science, Princess Nourah bint Abdulrahman University, Riyadh, Saudi Arabia*
[b] *Ural Federal University, St. Mira, 19, 620002 Yekaterinburg, Russia*
[c] *Nuclear Materials Authority, PO. BOX 530 El-Maadi, Cairo, Egypt*
[d] *Department of Physics, Faculty of Science, Isra University, Amman, Jordan*
[e] *Department of Nuclear Medicine Research, Institute for Research and Medical Consultations (IRMC), Imam Abdulrahman bin Faisal University (IAU), Dammam, Saudi Arabia*

ARTICLE INFO

Article history:
Received 10 January 2021
Accepted 7 May 2021
Available online 2 June 2021

Keywords:
Gamma-ray shielding
Monte Carlo simulation
BXCOM
Makishima–Makinze mode
Elastic properties

ABSTRACT

The substitution of La_2O_3 by Tb_2O_3 was studied for glass samples with a chemical composition described by: $75P_2O_5 + (25 - x)\ La_2O_3 + xTb_2O_3$, where x = 5, 10, 15, 20 mol%. The mechanical properties were predicted via the Makishima–Mackenzie model. The study demonstrated that when increasing the Tb_2O_3 content from 5 to 20 mol%, the elastic moduli of the glasses decreased, while the dissociation energy, packing density, and micro-hardness increased. In addition, the radiation shielding properties were studied using the MCNP5 code, which was utilized to simulate the linear attenuation coefficient (LAC) of the investigated samples. Furthermore, the mass attenuation coefficients (MAC) of the glasses were determined. The highest MAC was reported for the sample with 20 mol% of Tb_2O_3 and decreased from 0.358 to 0.0515 cm^2/g between 0.184 and 1.408 MeV. Furthermore, the effective atomic number (Z_{eff}), equivalent atomic number (Z_{eq}), exposure buildup factor (EBF), and the energy absorption buildup factor (EABF) of the glasses were calculated utilizing BXCOM software. The substitution of La_2O_3 by Tb_2O_3 was revealed to enhance the shielding features of the TLP samples.

* *Corresponding author.*
E-mail addresses: kmakhmud@urfu.ru, karemabdelazeem@yahoo.com (K. Mahmoud).
https://doi.org/10.1016/j.bsecv.2021.05.003

El papel de Tb_2O_3 en la mejora de las propiedades del sistema de vidrio La_2O_3-P_2O_5: estudio de blindaje mecánico y de radiación

Palabras clave:
Blindaje de rayos gamma
Simulación del Monte Carlo
BXCOM
Modo Makishima-Makinze
Propiedades elásticas

RESUMEN

Se estudió la sustitución de La_2O_3 por Tb_2O_3 para cinco muestras de vidrio con una composición química descrita por la fórmula: $75P_2O_5 + (25\text{-}x)\ La_2O_3 + xTb_2O_3$, donde x = 5, 10, 15 y 20% mol. Se evaluaron las propiedades mecánicas y de protección contra la radiación de las muestras de vidrio investigadas. Las propiedades mecánicas se predijeron utilizando el modelo de Makishima-Mackenzie. El estudio demostró que al aumentar el contenido de Tb_2O_3 de 5 al 20% en moles, los módulos elásticos (Young, Bulk, Shear y longitudinal) de los vidrios disminuyeron, mientras que aumentaron la energía de disociación, densidad de empaquetamiento y microdureza. Además, se estudiaron las propiedades de protección contra la radiación de las muestras de vidrio investigadas utilizando el código de transporte de partículas N de Monte Carlo (MCNP-5). Se utilizó MCNP-5 para simular el coeficiente de atenuación lineal (LAC) de las muestras investigadas. Con base en el LAC simulado, se determinaron los coeficientes de atenuación de masa (MAC) de las gafas. El MAC más alto se obtuvo para la muestra de vidrio con el 20% en moles de Tb_2O_3 y disminuyó de 0,358 a 0,0515 cm^2/g cuando se incrementó la energía del fotón gamma de 0,184 a 1,408 MeV. Además, el número atómico efectivo (Z_{eff}), el número atómico equivalente (Z_{eq}), el factor de acumulación de exposición (EBF) y el factor de acumulación de absorción de energía (EABF) de los vidrios se calcularon utilizando el software BXCOM. Se reveló que la sustitución de La_2O_3 por Tb_2O_3 mejora las propiedades de protección contra la radiación de las muestras investigadas.

Introduction

As technologies keep beneficent, a large number of equipment that depend on radiation and radioisotopes has been manufactured and used. The great use of these devices in which different ionizing radiation types are used extends from medical, industrial and agricultural applications and even we have become using any radiation devices in homes, hospitals, and research centers [1–4]. Direct exposure to radiation or even indirect radiation for relatively long periods of time leads to a set of health problems such as skin burns or various cancers. Thus, a human can be protected from the radiation using various materials like lead, glasses and so on [5,6]. Therefore, we find many protocols that have been developed to regulate the use of radiation in various facilities such as hospitals, research centers, and various medical facilities. These protocols focus on three essential points: diminishing the radiation exposure time and increasing the distance between the radioactive source and the person and, most importantly, the use of protective materials, which are called radiation shielding materials [7–10]. These materials can absorb the incoming radiation and thus decrease the radiation's intensity to safe levels.

Therefore, researchers in the field of nuclear engineering are trying to design different types of radiation protection materials according to the application in which these materials will be used, but in all cases, these materials must have a high ability to absorb the largest possible amount of radiation. For instance, in the past few years, researchers succeeded in developing alloys, ceramics, polymers, lead composite, glasses, and concrete as shielding materials [11–14].

Through these different kinds of materials, glass has attracted researchers as a promising material for radiation protection due to its excellent physical, chemical, and optical features. Glass is also easy to manufacture in several ways, available in abundance, and at a relatively cheap cost compared to other types of materials. Moreover, one of the most important advantages of glass that encourages researchers and radiation protection materials developers is the ease of controlling the density of glass using heavy element oxides. It is known that the density is an important factor that enhances the performance of the glass to absorb radiation and thus improve the radiation protection properties of the prepared glass [15–17].

Several kinds of glass formers are usually utilized to create the glass network. It is well known that changing the glass formers will fundamentally change the final glass system's features. P_2O_5, B_2O_3, and SiO_2 are typical glass formers that are used to fabricate phosphate, borate, and silicate glasses, respectively, and there are the earliest types of glasses and are still produced worldwide today [18,19]. Among several kinds of glasses, Phosphate glasses are featured compared to the traditional glasses, and this is due to some interesting features such as and high thermal expansion coefficient, high ultraviolet transmission, and low melting point [20]. Moreover, P_2O_5 has an excellent glass forming capability to dissolve high amounts of several types of glasses modifiers such as transition-metal, alkaline, and rare earth elements.

Previous studies on the possibility of using phosphate glass are still few and limited. Therefore, it is quite indispensable to examine the potential of utilizing phosphate glass as a new glass used in radiation protection. Thus, the mechanical properties and gamma-ray shielding capacity of

Table 1 – The chemical composition of the examined TLP samples.

Glass code	The chemical composition (Wt%)			Density	Molecular weight
	Tb_2O_3	La_2O_3	P_2O_5	g/m^3	g/mol
TLP5	5	20	75	3.1371	183.51
TLP10	10	15	75	2.9887	187.11
TLP15	15	10	75	2.9584	190.71
TLP20	20	5	75	2.9114	194.31

the $75P_2O_5 + (25 - x)La_2O_3 + xTb_2O_3$ glass system were studied. The Makishima–Mackenzie model was utilized to estimate the mechanical moduli of the examined samples. The MCNP-5 code was applied to simulate the radiation attenuation factors for the TLP samples

Materials and methods

Mechanical properties

In this work, the glass network's elastic properties with a chemical composition of $75P_2O_5 + (25 - x)La_2O_3 + xTb_2O_3$ are studied. TLP glasses are selected from reference [21]. Table 1 lists the nominal chemical composition and the density (ρ) of these TLP samples. Based on the packing coefficient (V_i) and dissociation energy (G_i) of the metal oxides constituting the TLP glasses, the mechanical moduli, such as Young's (Y), shear (S), Bulk (B), longitudinal (L), Poisson's ratio (μ) and micro-hardness (H) are detected [22–24]. According to the following equations, the dissociation energy (G_t) and packing density (V_t) can be calculated based on the ionic radius and the heat of formation of the constituting compounds.

$$G_t(\text{kJ cm}^{-3}) = \sum_i X_i G_i \quad (1)$$

$$V_t(\text{cm}^3\,\text{mol}^{-1}) = \frac{\rho}{M}\sum_i X_i V_i \quad (2)$$

where M represents the molecular weight of the examined TLP glasses.

$$Y = 2V_t G \quad (3)$$

$$B = 1.2V_t Y \quad (4)$$

$$S = \frac{3YB}{(9B - Y)} \quad (5)$$

$$L = B + \frac{3}{4}S \quad (6)$$

$$\mu = \frac{Y}{2S} - 1 \quad (7)$$

$$H = \frac{(1 - 2\mu)}{6(1 + \mu)} \quad (8)$$

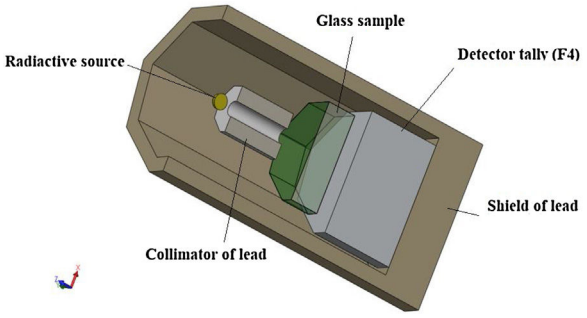

Fig. 1 – The geometry utilized in the simulation processes.

Gamma-ray shielding features

The MCNP-5 code is a simulation program used to detect shielding features [25]. The input file used to examine the photon attenuation competence for the TLP glasses is exhibited in Fig. 1. The details about the input file is mentioned in our work [26]. The identified sources in this investigation are ^{60}Co with 1.173 and 1.332 MeV energy, ^{137}Cs with 0.662 MeV energy, and ^{106}Ho 0.184 and 0.28 MeV energy, respectively. In order to assess the average track length (ATL) of the incident photons in the tested TLP samples, the detector was presumed to be an F4 tally. Based on the ATL, some shielding parameters like the mass and linear attenuation coefficients (we will use the abbreviations MAC and LAC for these two quantities) were simulated. The simulated results of these two quantities were then utilized to predict further important quantities, such as mean free path (MFP) and transmission rate (TR) [26–28].

$$LAC(\text{cm}^{-1}) = \frac{1}{x}\ln\left(\frac{I_o}{I}\right) \quad (9)$$

$$\mu_m\left(\frac{\text{cm}^2}{\text{g}}\right) = \frac{LAC\,(\text{cm}^{-1})}{\rho\,(\text{g cm}^{-3})} \quad (10)$$

$$TF\,(\%) = \frac{I}{I_o} = \exp^{(-LAC*x)} \quad (11)$$

$$MFP\,(\text{cm}) = \frac{1}{LAC\,(\text{cm}^{-1})} \quad (12)$$

The I_o and I denote the incoming and transmitted photon intensities. Where x represents the thickness of the sample.

The recent BXCOM software was used for the evaluation of the effective and equivalent atomic numbers (Z_{eff} and Z_{eq}). Also, it helped for the evaluation of the buildup factors for the examined TLP specimens [29].

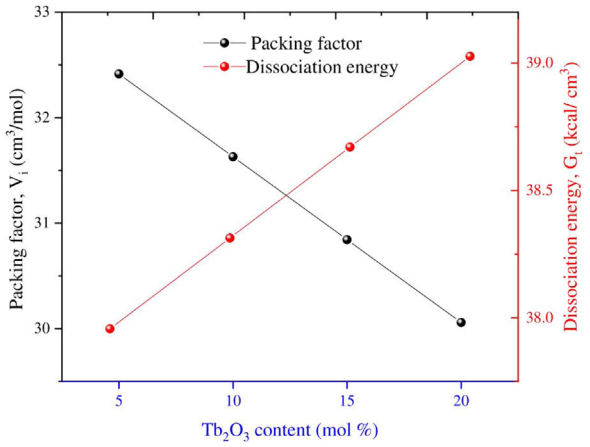

Fig. 2 – Variation of packing factor V_i and dissociation energy G_t associated with substitution of La_2O_3 by Tb_2O_3 content.

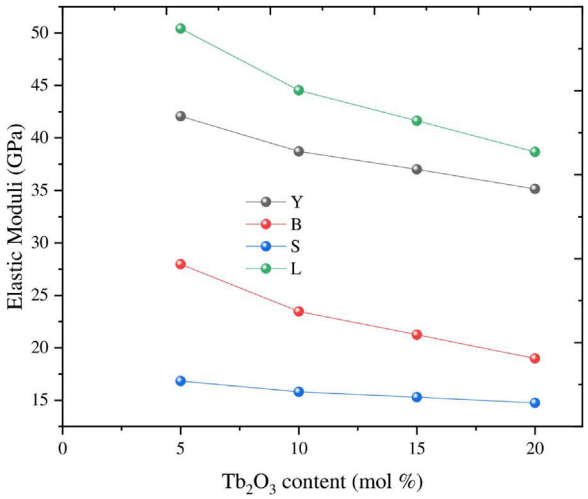

Fig. 3 – The elastic moduli (Longitudinal, Young, Shear, and Bulk) as a function of Tb_2O_3.

Results and discussion

Elastic properties

The Makshima–Makenzie model was used to determine the mechanical parameters of the fabricated TLP samples based on the Pauli ionic radius and the heat of formation (ΔH_f) of each compound. Fig. 2 illustrates that the fabricated TLP glass samples' packing factor (V_i) reduced from 32.415 to 29.273 cm^3/mol for TLP5 (with 5 mol%) and TLP20 (with 20 mol%) of the Tb_2O_3 content. This attributed to the replacement of La with a highly ionic radius (R_{La} = 1.032 Å) by Tb with a lower ionic radius (R_{Tb} = 0.923 Å). Fig. 2 also shows that the dissociation energy G_t increased from 37.957 to 39.384 kcal/cm^3 with increasing the Tb_2O_3 concentration between 5 and 20 mol%, respectively. The mentioned increase in the G_t is due to the substitution of La_2O_3 with dissociation energy (G_i = 65.8 kcal/cm^3) by Tb_2O_3 content with dissociation energy (G_i = 72.934 kcal/cm^3).

Based on the calculated G_t and V_i values, the mechanical moduli (Young, Longitudinal, Shear, and Bulk) were also predicted. Fig. 3 depicts the elastic moduli versus the Tb_2O_3 substitution ratio. The elastic model (*E*) decreased from 42.063 to 31.637 GPa, Bulk (*B*) model reduced from 27.969 to 15.248 GPa, Shear (S) declined from 16.834 to 13.705 GPa, and Longitudinal (*L*) model decreased from 50.414 to33.521 GPa with increasing the Tb_2O_3 substitution ratio from 5 to 20 mol%. These reductions are due to the La—O bonds' replacement with high bond stretch and formation energy with a new Tb—O bond.

As mentioned in Eq. (9), the Poisson ratio was calculated. The Poisson ratio takes values 0.249, 0.225, 0.210, 0.192, and 0.154 for glass samples TLP5, TLP10, TLP15, and TLP20, respectively. Fig. 4 illustrates the Poisson ratio's reduced with

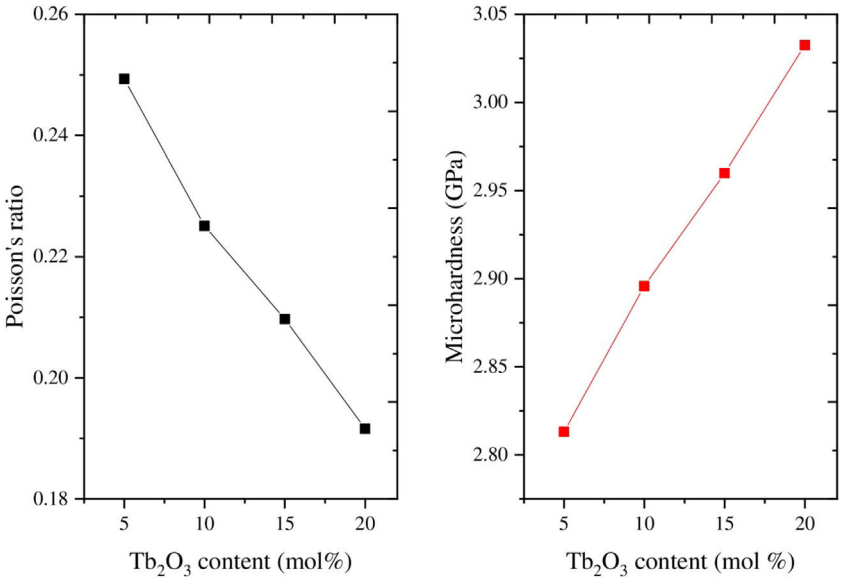

Fig. 4 – The Poisson ratio and Micro-hardness as a function of Tb_2O_3 content.

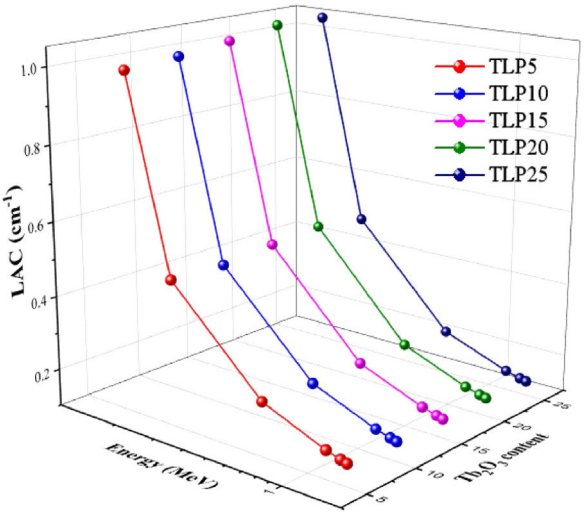

Fig. 5 – The LAC as a function of energy and Tb_2O_3 content.

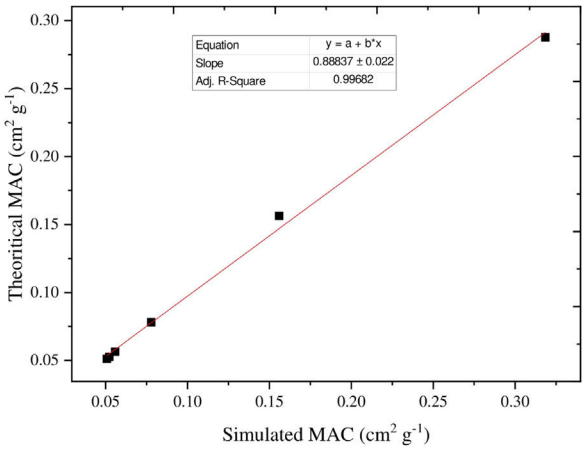

Fig. 6 – Correlation between the XCOM and MCNP-5 values for TLP5 sample.

increasing the Tb_2O_3 between 0 and 20 mol%. The mentioned reduction is due to the detected decrease in the packing density V_i and Young model (E).

Hardness is an essential mechanical feature widely utilized to predict a material's ability to withstand an input load. It is divided into microhardness and macro hardness. Glass samples are usually smaller and thinner. Therefore, in the current work, the study of microhardness (H) is more important. The data in Fig. 4 and Table 2 showed that the micro-hardness varied between 2.813, 2.896, 2.960, and 3.033 GPa for glass samples TLP5, TLP10, TLP15, and TLP20 glass samples.

Radiation shielding properties

Fig. 5 displays the LAC for the TLP glasses. According to this figure, the LAC is affected by the incident energy. Also, it is affected by composition of the TLP glass. The highest LAC is found 0.184 MeV, and increases from 0.99 to 1.024 cm^{-1} for TLP5 with 5 mol % and TLP 20 with 20 mol%, respectively. It was also observed that with increasing the incoming radiation energy, the simulated LAC values decreased due to Compton scattering interaction (CS) [30]. The lowest LAC values were reported at 1.408 MeV and equal to 0.159 cm^{-1} for TLP5 and 0.149 cm^{-1} for TLP20.

The LAC was also affected by the chemical composition of the TLP glasses. The molecular weight of phosphate glass affected increases with the insertion of Tb_2O_3. Therefore, Z_{eff} progressively falls, decreasing by increasing the molecular weight of TLP glasses. The lowest LAC was observed at TLP5 with 5% mol Tb_2O_3 and suddenly increased to higher values for the TLP20 with 20% mol Tb_2O_3. The TLP20 has higher LAC values than TLP5, TLP10, and TLP15, respectively. The LAC values for TLP5 glass decrease from 0.99 to 0.159 cm^{-1} and for TLP20 glass from 1.044 to 0.149 cm^{-1} between 0.184 and 1.408 MeV. The LAC is found to increase with the insertion of Tb_2O_3 into the phosphate specimens. The previous trend in the LAC is related to the CS.

Additionally, the MAC can be estimated based on the values of simulated LAC for TLP glasses. The MAC's simulated values were compared with the theoretical MAC values, which were determined from the XCOM software. The strong correlation between the two approaches used to evaluate the MAC for the chosen TLP5 glass and is introduced in Fig. 6. We also found good agreement for all the remaining samples and a strong correlation between the MAC obtained from the two approaches. The difference (%) between the simulated and theoretical MAC was detected via the following Eq. (13) and documented in Table 3:

$$Diff(\%) = \frac{\left[(\mu_m)_{mcnp} - (\mu_m)_{xcom}\right]}{(\mu_m)_{mcnp}} \times 100\% \quad (13)$$

The difference (%) was found lower than 10% for the TLP5, TLP10, TLP15 and TLP20 glasses.

The transmission rate (TF) of incident gamma radiation through the investigated glass material was studied and presented in Fig. 7. The transmission rate is an indicator of the number of incident gamma radiation interactions with the glass materials. Therefore, Fig. 7 illustrates the variation of TR values with the incident gamma energy and the thickness of TLP glasses. First, At the same thickness of the investigated TLP glass, the TR varies linearly with the incident gamma energy. The highest values of TR were observed at high energies (1.408 MeV) and decrease from 0.85 to 0.45 for TLP5 and diminishing from .0.86 to 0.47 While at low incident gamma energy (0.184 MeV), the TR has low values and decrease from 0.37 to 0.007 for TLP5, and from 0.35 to 0.005 for TLP20. The transmission rate of incident gamma depends on the interactions inside the glass material, which led to a decrease in the gamma wavelength. Thus, the number of interactions of the gamma radiation decrease and can be penetrated the glass material. Therefore, the TF of incident gamma radiation increases. The second main factor is the thickness of TLP glasses. The variation of TR with the thickness of TLP glasses was presented in Fig. 7. The transmission rate at incident gamma energy (0.184 MeV) decreases from 0.37 to 0.007 for TLP5 glass with thickness of 1 and 5 cm, respectively. The increasing of the specimen's thickness leads to the TR of incident gamma radiation decrease. This is because the

Table 2 – Different mechanical parameters for the examined samples.

Glass sample	V_i (cm^3/mol)	G_t (kcal/cm^3)	V_t (cm^3/mol)	E (GPa)	B (GPa)	S (GPa)	μ	H (GPa)	L (GPa)	V_l (m/s)	V_s (m/s)
TLP5	32.415	37.957	0.554	42.06374	27.969	16.834	0.2493	2.813	50.414	4008.871	2316.544
TLP10	31.629	38.313	0.505	38.712	23.469	15.800	0.225	2.896	44.535	3860.200	2299.236
TLP15	30.844	38.670	0.478	37.00357	21.245	15.294	0.210	2.960	41.638	3751.591	2273.722
TLP20	30.059	39.027	0.450	35.152	18.997	14.750	0.192	3.033	38.664	3644.182	2250.832

Table 3 – The simulated (MCNP-5) and XCOM MAC for the examined samples.

Glass sample	Mass attenuation coefficient (cm^2/g)											
	TLP5			TLP10			TLP15			TLP20		
E (MeV)	MCNP-5	XCOM	Difference (%)	MCNP-5	XCOM	Difference (%)	MCNP-5	XCOM	Difference (%)	MCNP-5	XCOM	Difference (%)
0.184	0.3185	0.2877	9.6644	0.3374	0.3059	9.3317	0.3462	0.3236	6.5226	0.3585	0.3410	4.8939
0.28	0.1560	0.1563	−0.2036	0.1619	0.1623	−0.2340	0.1677	0.1681	−0.2173	0.1734	0.1739	−0.2712
0.662	0.0779	0.0780	−0.2021	0.0785	0.0787	−0.2172	0.0792	0.0794	−0.2373	0.0798	0.0800	−0.2462
1.173	0.0558	0.0564	−1.0751	0.0560	0.0566	−1.1316	0.0561	0.0568	−1.1935	0.0562	0.0569	−1.2423
1.332	0.0522	0.0527	−0.9088	0.0523	0.0528	−0.9505	0.0524	0.0530	−0.9952	0.0525	0.0531	−1.0436
1.408	0.0508	0.0512	−0.8084	0.0509	0.0513	−0.8459	0.0510	0.0514	−0.8880	0.0511	0.0515	−0.9335

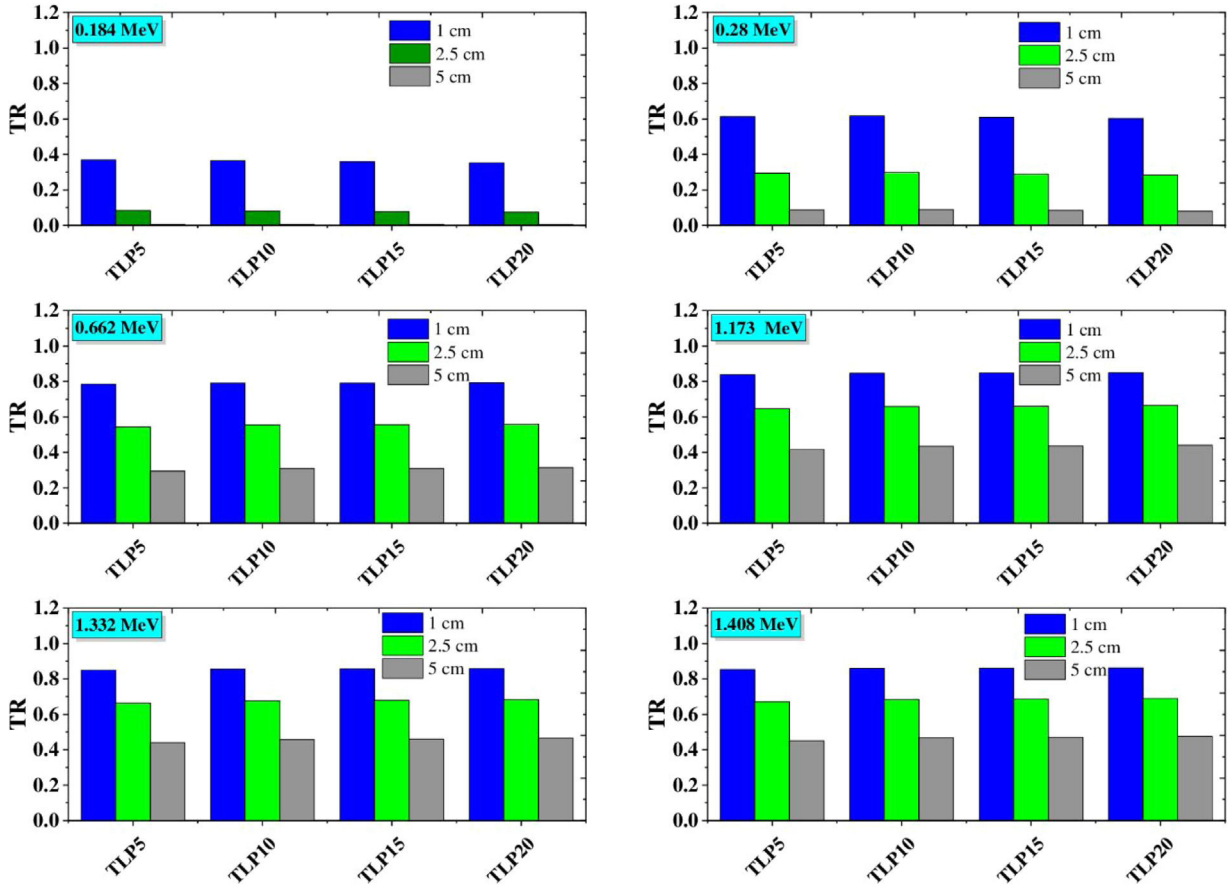

Fig. 7 – The transmission ratio (TF) variation as a function of the glass thickness.

photons will spend more time passing through the glass material, and the number of incident gamma interactions with glass materials increase.

Fig. 8 depicts the mean free path for the TLP5, TLP10, TLP15 and TLP20 glasses. Also, in the same figure, the MFP for the aforementioned glasses is compared with the RS-253-G18 glass as well as the previously borax glass 40%. Fig. 8 displays the MFP of TLP glasses increases with increasing the energy. The highest and lowest MFP was found at 1.408 MeV and 0.18 MeV, respectively. The values of MFP for the TLP glasses are lower than Borax 40% and the RS-253-G18. Therefore, the TLP glasses are convenient high-density shielding glass.

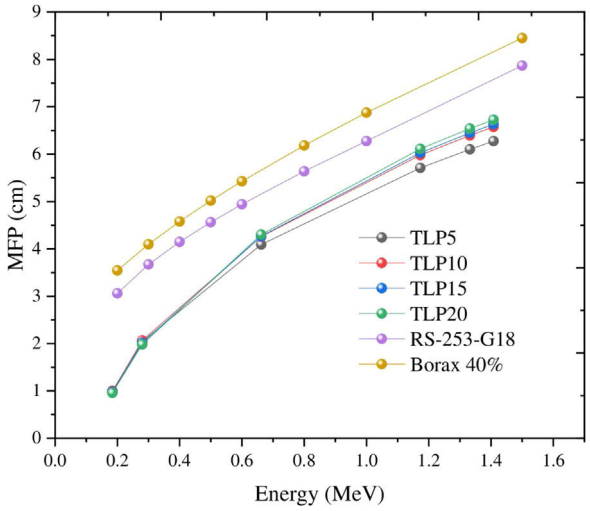

Fig. 8 – The MFP of the TLP glasses in comparions with other previously prepared glass samples.

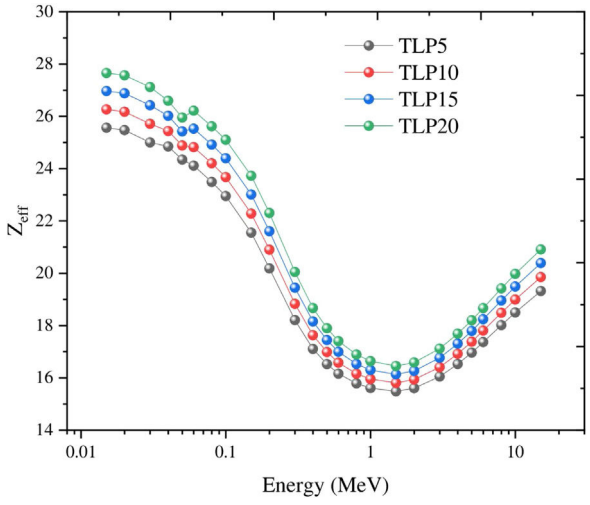

Fig. 9 – The effective atomic number (Z_{eff}) for the TLP samples.

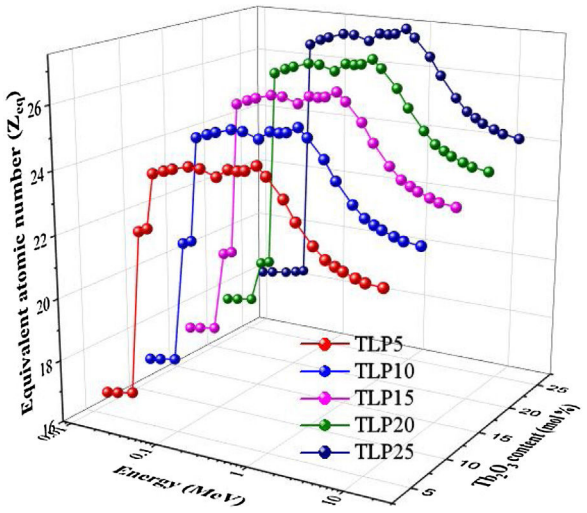

Fig. 10 – The equivalent atomic number (Z_{eq}) for the TLP samples.

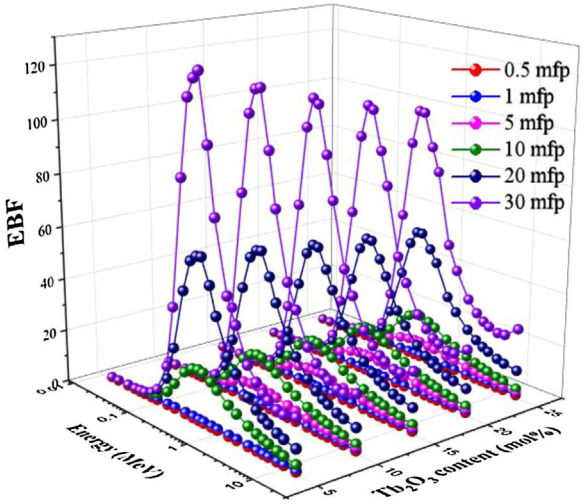

Fig. 11 – The exposure buildup factor (EBF) for the TLP samples.

In this study, the other shielding parameters such as Z_{eff}, Z_{eq}, EBF, and EABF were reported via the BXCOM program database in the range of incident gamma energies (0.015–15 MeV). Fig. 9 illustrates the Z_{eff} for the tested TLP glasses. At low energies (<0.1 MeV), the photoelectric effect (PE) is the prevalent process, with increasing the incident gamma energy, the Z_{eff} values found drop progressively decrease, but can observe unexpected peaks at 0.0552 MeV. After that, the Compton scattering interaction (CS) was observed at an energy range (>0.1–1 MeV). The Compton scattering reduces with increasing the incident energy. This is attributed from the cross-section of CS where ($\sigma_{CS} \propto E^{-1}$). Then it can be observed that the Z_{eff} was raised with increasing the incident gamma energy above 1 MeV.

Fig. 10 represents the changes in the Z_{eq} versus the incident energy for the TLP samples. The smallest Z_{eq} is achieved at energies lower than 0.1 MeV, where the PE region. Then, the Z_{eq} values increased gradually with increasing the energy where the CS region was started. Then Z_{eq} values speedily decrease with increasing the energies in the PP region.

Two building factors that can describe photons' accumulation inside the materials of TLP glasses are the exposure building factor (EBF) and the energy absorption building factor (EABF). Figs. 11 and 12 exhibit how the buildup factors change with the incident gamma energy, penetration depth in mfp unit, and the content of Tb_2O_3 for the TLP glasses. The EBF and EABF have low in the PE region, where the incident gamma's energy removes all incident gamma photons. Then, both factors given in Figs. 11 and 12 increase with increasing the energy. The CS interaction inside TLP glasses' material increases and a small part of the incident photons passes through the material. Hence the rest part of the incident photons produce scattered photons that accumulated inside the

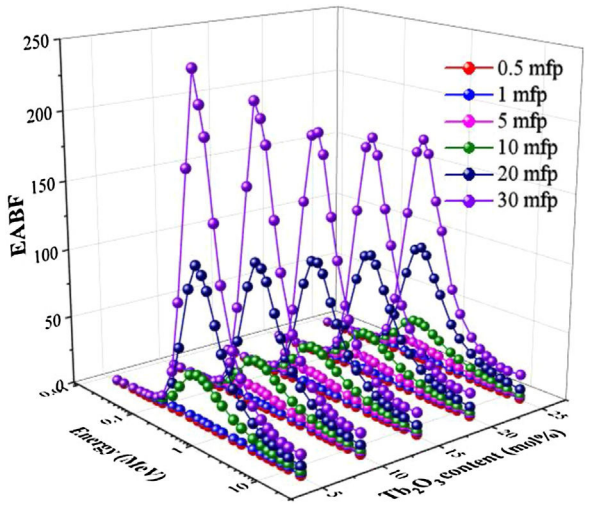

Fig. 12 – The energy absorption buildup factor for the TLP samples.

investigated glass material. For $E > 1.5$ MeV, the PP interactions are dominant.

Furthermore, the EBF and EABF were raised regularly by increasing the PD up to 30 mfp. The photons spent more time to pass through the thickness material of TLP glasses. Thus, the more interactions will produce, and the photons accumulation will increase inside the TLP samples. The highest values were noticed at high penetration depth PD (PD = 30 mfp), while the lowest values were detected at 0.5 mfp.

Figs. 11 and 12 display the variation of estimated EBF and EABF values with the insertion of the Tb_2O_3 content in the examined glasses. Apparently, both factors are diminish gradually with the increment of the Tb_2O_3 content (mol%) in the TLP glasses. The highest and lowest EBF and EABF are achieved at 5 and 20 mol% of Tb_2O_3. Where the insertion of Tb_2O_3 content in the TLP glasses don't leads to accumulate the photons in the examined glasses at the high content of Tb_2O_3.

Conclusion

The role of Tb_2O_3 on the mechanical and radiation protection characteristics was studied for $75P_2O_5 + (25 - x)La_2O_3 + xTb_2O_3$ glass systems. The results revealed that the dissociation energy (G_t) changes between 37.95 and 39.38 kcal/cm^3 with increasing the Tb_2O_3 substitution ratio between 5 and 20 mol%. The packing density(V_t), Young's (E), shear (S), Bulk (B), and Longitudinal (L) moduli decreased between 0.554–0.402 cm^3/mol, 42.06–31.36 Gap, 27.96–15.24 GPa, 16.83–13.70 GPa, and 50.41–33.54 GPa, respectively. The shielding capacity against gamma-photons was evaluated using the MCNP-5 code between 0.184 and 1.408 MeV. The best MAC achieved for the investigated glass sample TPL20 varied between 0.358 and 0.0515 cm^2/g in the examined energy range. The replacement of La_2O_3 with Tb_2O_3 results in an enhancement in the MAC values by 11.03% at 0.184 MeV. The highest and lowest MFP was found at 1.408 MeV and 0.18 MeV, respectively. The values of MFP for the TLP glasses are lower than Borax 40% and the RS-253-G18. Moreover, the highest values of TR were observed at high energies (1.408 MeV) and decrease from 0.85 to 0.45 for TLP5 and diminishing from .0.86 to 0.47. While at low incident gamma energy (0.184 MeV), the TR has low values and decrease from 0.37 to 0.007 for TLP5 and from 0.35 to 0.005 for TLP20.

Acknowledgments

This research was funded by the Deanship of Scientific Research at Princess Nourah bint Abdulrahman University through the Fast-track Research Funding Program to support publication in the top journal (Grant no. 42-FTTJ-22).

REFERENCES

[1] S. Yasmin, B.S. Barua, M.U. Khandaker, M.A. Rashid, D.A. Bradley, M.A. Olatunji, M. Kamal, Studies of ionizing radiation shielding effectiveness of silica-based commercial glasses used in Bangladeshi dwellings, Results Phys. 9 (2018) 541–549.
[2] H. Akyildirim, E. Kavaz, F.I. El-Agawany, E. Yousef, Y.S. Rammah, Radiation shielding features of zirconolite silicate glasses using XCOM and FLUKA simulation code, J. Non-Cryst. Solids 545 (2020) 120245.
[3] Y. Al-Hadeethi, M.I. Sayyed, Y.S. Rammah, Fabrication, optical, structural and gamma radiation shielding characterizations of GeO_2–PbO–Al_2O_3–CaO glasses, Ceram. Int. 46 (2020) 2055–2062.
[4] S. Yasmin, Z.S. Rozaila, M.U. Khandaker, B.S. Barua, F.U.Z. Chowdhury, M.A. Rashid, D.A. Bradley, The radiation shielding offered by the commercial glass installed in Bangladeshi dwellings, Radiat. Eff. Defects Solids 173 (7–8) (2018) 657–672.
[5] S. Shamsan Obaid, K. Dhammajyot Gaikwad, P. Pravina Pawar, Determination of gamma ray shielding parameters of rocks and concrete, Radiat. Phys. Chem. 144 (2018) 356–360.
[6] M. Dong, X. Xue, H. Yang, Z. Li, Highly cost-effective shielding composite made from vanadium slag and boron-rich slag and its properties, Radiat. Phys. Chem. 141 (2017) 239–244.
[7] M. Dong, X. Xue, H. Yang, D. Liu, C. Wang, Z. Li, A novel comprehensive utilization of vanadium slag: as gamma ray shielding material, J. Hazard. Mater. 318 (2016) 751–757.
[8] M.H.A. Mhareb, Physical, optical and shielding features of Li_2O–B_2O_3–MgO–Er_2O_3 glasses co-doped of Sm_2O_3, Appl. Phys. A 126 (2020) 71.
[9] S. Kaewjaeng, S. Kothan, W. Chaiphaksa, N. Chanthima, R. Rajaramakrishna, H.J. Kim, J. Kaewkhao, High transparency La_2O_3–CaO–B_2O_3–SiO_2 glass for diagnosis X-rays shielding material application, Radiat. Phys. Chem. 160 (2019) 41–47.
[10] M. Dong, X. Xue, S. Liu, H. Yang, Z. Li, M.I. Sayyed, O. Agar, Using iron concentrate in Liaoning province, China, to prepare material for X-ray shielding, J. Cleaner Prod. 210 (2019) 653–659.
[11] R. Bagheri, A.K. Moghaddam, S.P. Shirmardi, B. Azadbakht, M. Salehi, Determination of gamma-ray shielding properties for silicate glasses containing Bi_2O_3 PbO, and BaO, J. Non-Cryst. Solids 479 (2018) 62–71.
[12] A.H. El-Kateb, R.A.M. Rizk, A.M. Abdul-Kader, Determination of atomic cross-sections and effective atomic numbers for some alloys, Ann. Nucl. Energy 27 (2000) 1333–1343.
[13] H.C. Manjunatha, L. Seenappa, B.M. Chandrika, C. Hanumantharayappa, A study of photon interaction parameters in barium compounds, Ann. Nucl. Energy 109 (2017) 310–317.

[14] H.C. Manjunatha, L. Seenappa, B.M. Chandrika, K.N. Sridhar, C. Hanumantharayappa, Gamma, X-ray and neutron shielding parameters for the Al-based glassy alloys, Appl. Radiat. Isotope. 139 (2018) 187–194.
[15] Y.S. Alajerami, D. Drabold, M.H.A. Mhareb, K.L.A. Cimatu, G. Chen, M. Kurudirek, Radiation shielding properties of bismuth borate glasses doped with different concentrations of cadmium oxides, Ceram. Int. 46 (2020) 12718–12726.
[16] Y. Al-Hadeethi, M.I. Sayyed, H. Mohammed, L. Rimondin, X-ray photons attenuation characteristics for two tellurite based glass systems at dental diagnostic energies, Ceram. Int. 46 (2020) 251–257.
[17] R. Kurtulus, T. Kavas, I. Akkurt, K. Gunoglu, An experimental study and WinXCom calculations on X-ray photon characteristics of Bi_2O_3- and Sb_2O_3-added waste soda-lime-silica glass, Ceram. Int. 46 (2020) 21120–21127.
[18] Y. Al-Hadeethi, M.I. Sayyed, BaO–Li_2O–B_2O_3 glass systems: potential utilization in gamma radiation protection, Prog. Nuclear Energy 129 (2020) 103511.
[19] A.M. Ibrahim, Impact of MoO_3 concentration, frequency and temperature on the dielectric properties of zinc phosphate glasses, Chin. J. Phys. 68 (2020) 919–929.
[20] Z. Černošek, J. Holubová, P. Hejda, The influence of phosphorus substitution by molybdenum on the chemical composition and certain properties of the zinc metaphosphate glass, J. Non Cryst. Solids 522 (2019) 119556.
[21] A. Babkina, E. Kulpina, Y. Sgibnev, Y. Fedorov, A. Starobor, O. Palashov, N. Nikonorov, A. Ignatiev, K. Zyryanova, K. Oreshkina, E. Zhizhin, D. Pudikov, Terbium concentration effect on magneto-optical properties of ternary phosphate glass, Opt. Mater. 100 (2020) 109692.
[22] S. Inaba, S. Fujino, K. Morinaga, Young's modulus and compositional parameters of oxide glasses, J. Am. Ceramic Soc. 82 (1999) 3501–3507.
[23] A. Makishima, J.D. Mackenzie, Direct calculation of Young's modulus of glass, J. Non-Cryst. Solids 12 (1973) 35–45.
[24] A. Makishima, J.D. Mackenzie, Calculation of bulks modulus, shear modulus and Piosson's ratio of glass, J. Non-Cryst. Solids 17 (1975) 147–157.
[25] X-5 Monte Carlo Team, MCNP-A General Monte Carlo N-Particle Transport Code, Version 5 Los Alamos Controlled Publication. LA-CP-03-0245, 2003.
[26] K.A. Mahmoud, E. Lacomme, M.I. Sayyed, Ö.F. Özpolat, O.L. Tashlykov, Investigation of the gamma ray shielding properties for polyvinyl chloride reinforced with chalcocite and hematite minerals, Heliyon 6 (2020) e03560.
[27] K.M. Kaky, M.I. Sayyed, A.A. Ali, M.H.A. Mhareb, K.A. Mahmoud, S.O. Baki, Germanate oxide impacts on the optical and gamma radiation shielding properties of TeO_2–ZnO–Li_2O glass system, J. Non-Cryst. Solids 546 (2020) 120272, http://dx.doi.org/10.1016/j.jnoncrysol.2020.120272.
[28] M.I. Sayyed, K.A. Mahmoud, S. Islam, O.L. Tashlykov, E. Lacomme, K.M. Kaky, Application of the MCNP 5 code to simulate the shielding features of concrete samples with different aggregates, Radiat. Phys. Chem. (2020) 108925, http://dx.doi.org/10.1016/j.radphyschem.2020.108925.
[29] Ö. Eyecioğlu, A.M. El-Khayatt, Y. Karabul, M. Çağlar, O. Toker, O. İçelli, BXCOM: a software for computation of radiation sensing, Radiat. Effects Defects Solids 174 (2019) 506–518, http://dx.doi.org/10.1080/10420150.2019.1606811.
[30] R. El-mallawany, M.I. Sayyed, M.G. Dong, Y.S. Rammah, Simulation of radiation shielding properties of glasses contain PbO, Radiat. Phys. Chem. 151 (2018) 239–252, http://dx.doi.org/10.1016/j.radphyschem.2018.06.035.